Fe/Cr interface magnetism: Correlation between hyperfine fields and magnetic moments

V. M. Uzdin
ICAPE, Saint-Petersburg State University, V.O. 14 Linia 29, 199178, St. Petersburg, Russia

W. Keune, H. Schrör, and M. Walterfang
Laboratorium für Angewandte Physik, Gerhard-Mercator-Universität Duisburg, Lotharstr. 65, D-47048 Duisburg, Germany
(Received 28 February 2000; revised manuscript received 14 November 2000; published 14 February 2001)

The magnetic hyperfine field (hff) in epitaxial Fe/Cr(001) superlattices on Mg(001) with different thicknesses of interfacial ^{57}Fe probe layers was measured by Mössbauer spectroscopy. Self-consistent calculations of the Fe and Cr atomic magnetic moments in the interface region were performed within the periodic Anderson model for the same superlattice structure. Different kinds of interface roughness/interdiffusion were modeled using special algorithms. For every kind of interface roughness the distribution of local magnetic moments among the Fe atoms with a given number of nearest and next-nearest Cr neighbors was calculated. We obtain a strong correlation between the experimental hff and calculated local Fe magnetic moments. Peak positions in the hff distribution and correlated positions of maxima in the distribution function for local magnetic moments are observed to be stable relative to changes in the alloylike interface roughness. We found that the hff of ~20 T must correspond to interdiffused Fe atoms inside the Cr spacer layers a few atomic layers away from the ideal interface, contrary to earlier interpretations of Fe atoms at the atomically ''flat'' interface. As a measure of the Fe-Cr interface roughness on an atomic scale our results suggest an enhanced hff in the second Fe layer below the ideal interface in case of atomically smooth interfaces with large flat terraces.

DOI: 10.1103/PhysRevB.63.104407 PACS number(s): 75.70.Cn, 76.80.+y, 73.40.Jn

I. INTRODUCTION

Fe/Cr overlayers, sandwiches, and magnetic superlattices are the classical systems where recently a number of new phenomena important both for understanding of the nature of low-dimensional magnetism and for application in microelectronics have been discovered.[1] Among these new phenomena are short- and long-range oscillations of exchange coupling, giant magnetoresistance (GMR), and noncollinear magnetic ordering in the superlattices. It is well established now that most of the properties of the Fe/Cr systems crucially depend on the interface structure on an atomic scale, which is determined by the very delicate conditions of the sample preparation: temperature during the epitaxial growth, quality of the substrate, etc. Spatial defects (steps at the interface, embedded atoms and clusters of Fe in Cr and Cr in Fe, pinhole defects), which cannot be avoided during sample preparation, not only modify the magnetic characteristics of the whole system but often prove to be responsible for the new properties, being of large practical importance. According to Ref. 2 the bilinear exchange coupling in Fe/Cr trilayers can be changed by as much as a factor of 5 by varying the substrate temperature during the growth of the first Cr atomic layer. *In situ* magnetometry measurements demonstrated a very large decrease of the macroscopic (integral) moment during Cr evaporation on smooth Fe surfaces, whereas for rough Fe surfaces no change of the integral moment was observed at all.[3] All the theories of noncollinear magnetic ordering in Fe/Cr systems[4] presuppose the existence of spatial defects, which are the real reason for noncollinear structure formation. Therefore, investigation of roughness, interdiffusion, their dependence on the growth condition, and the control of the interface structure using different experimental methods became one of the principal topics for the Fe/Cr systems.

Most of the experimental techniques give only indirect information about chemical and magnetic roughness of the interfaces on an atomic scale. Averaging over the whole interface region or even on several interfaces in multilayers makes it difficult to reconstruct the microscopic interface structure from the experimental data. Only recently several experimental approaches were reported that allow to find the layer-by-layer distribution of Cr and Fe atoms for a Cr overlayer on the Fe surface. Scanning tunneling microscopy (STM) investigations, in combination with tunneling spectroscopy, showed the formation of an interfacial Cr-Fe alloy that is observed as a distribution of single atomic Cr impurities dispersed in the Fe substrate in the submonolayer-coverage regime,[5] or $Fe_{50}Cr_{50}$ surface alloy formation of submonolayer Fe on Cr(001) after annealing.[6] Proton- and electron-induced Auger-electron spectroscopy[7] and angular resolved Auger electron studies[2,8] also unambiguously confirmed the presence of interface alloying during growth of Cr on Fe. However, all of these methods work only for a Cr coverage of less than a few monolayers, and they cannot give information about the magnetic roughness associated with the chemical roughness of the interface. Quantitative atomically resolved information on magnetic moments near the interface may be derived, in principle, from an analysis of magnetic hyperfine fields (hff) that are obtained, in particular, by using Mössbauer spectroscopy.[9–16] By introducing a 1 to 2-monolayer (ML)-thick ^{57}Fe probe layer at the Fe/Cr interface, one can obtain local information about the distribution $P(B_{hf})$ of the hff in this region. The existence of ^{57}Fe atoms with various magnetic moments and with different local environments near the Fe/Cr interface leads to the appearance of satellite lines in the Mössbauer spectra. How-

ever, the interpretation of these data for low-dimensional Fe/Cr structures is very complicated and an ambiguous problem. The total hff can be conveniently decomposed into the contribution from the valence ($4s$) electrons and into the contribution from the core electrons, polarized by the localized magnetic moment on a given ^{57}Fe atom. For the bulk materials it is generally accepted that the hff scales approximately with the magnetic moment.[17] For surfaces, interfaces, and multilayers such an approach can be applied only for the core contribution, whereas the $4s$ part has to be investigated separately in every concrete case.[17]

Surprisingly, for most of the Fe/Cr multilayer structures the spectral positions of satellite Mössbauer lines do not differ very much,[9–16] although all other characteristics like GMR, parameters of exchange coupling, etc., as a rule, are very different. Comparison of hff distributions for Fe-Cr interfaces in the multilayers and for the Fe-Cr random alloys has led to the conclusion that as a first approach the interface region can be considered as a bulk alloy with varying concentration. For the treatment of Mössbauer spectra most investigations follow the empirical procedure, which was suggested initially for the description of random alloys.[18] The hff, B_{hf}, on the Fe atoms is assumed to decrease linearly in magnitude with the number of the nearest neighbor (n_1) and next-nearest neighbor (n_2) Cr atoms:

$$B_{\mathrm{hf}} = B_{\mathrm{hf}}(\mathrm{bulk}) + n_1 B_1 + n_2 B_2, \qquad (1)$$

where B_1 (B_2) is the contribution to the hff from one Cr atom in the first (second) shell around the Fe atom under consideration. Improvement of the resolution of the measurements and development of the epitaxial growth techniques offered the opportunity to refine the alloy model. For the description of the set of hff, Klinkhammer *et al.*[10] suggested the following relation:

$$B_{\mathrm{hf}} = B_{\mathrm{hf}}(\mathrm{bulk}) + n_1 B_1 + n_2 B_2 + \Delta B + \Delta B_{(i=2)}. \qquad (2)$$

Besides, of the fitting parameters $B_1 = 2.5$ T and $B_2 = 2.05$ T, which give the hff changes per Cr neighbor similar to the simple alloy approach of Eq. (1), this relation contains two additional parameters: $\Delta B = -1.75$ T, which the authors[10] connected with the broken spatial symmetry in the transverse direction; and $\Delta B_{(i=2)} = -1.2$ T, when ($n_1 = 0$, $n_2 = 1$) and equal to zero otherwise. Note, that $n_1 = 0$, $n_2 = 1$ corresponds to an Fe atom in the second atomic Fe layer below the ideal Fe/Cr interface. Taking into account that B_{hf} (bulk) is negative (-33.3 T at room temperature), we obtain from Eq. (2) an enhancement of the magnitude of B_{hf} for these atoms. Such an enhancement was detected experimentally only for molecular-beam grown epitaxial samples with smooth interfaces,[10,12] and was never reported for sputtered multilayers.[11,15,16]

Figure 1 illustrates schematically the distribution of discrete hff values that were obtained for Fe/Cr interfaces by different groups using conversion electron Mössbauer spectroscopy (CEMS). We underline again that the enhanced hff in the subsurface Fe layer exists only for smooth interfaces, and that its intensity is larger for those cases where interdiffusion is minimized or suppressed, e.g., like in the case of a

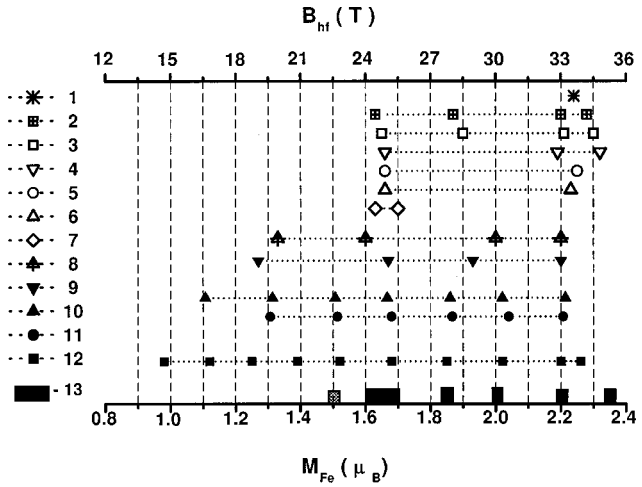

FIG. 1. Distribution of hff peak positions in Fe/Cr structures (upper abscissa). The ^{57}Fe-probe-layer thickness is underlined. Hatched square with cross at $1.5\mu_B$: calculated local Fe moment antiparallel to overall magnetization direction. 1—$W(110)$/Cr(110): 40 ML/Fe(110):3 ML+2 ML+21 ML+2 ML +3 ML/Cr(110) (Ref. 12); 2—$W(110)$/Cr(110): 40 ML/Fe(110):3 ML+25 ML+3 ML/Cr(110) (Ref. 12); 3—$W(110)$/Cr(110):40 ML/Fe(110):3 ML+4 ML+3 ML/Cr(110) (Ref. 12); 4—$W(110)$/Cr(110):40 ML/Fe(110):6 ML/Cr(110), (Ref. 12); 5—$W(110)$/Cr(110):40 ML/Fe(110):4 ML/Cr(110), (Ref. 12); 6—$W(110)$/Cr(110):40 ML/Fe(110):3.3 ML/Cr(110), (Ref. 12); 7—$W(110)$/Cr(110):40 ML/Fe(110):2 ML/Cr(110), (Ref. 12); 8—Si/Fe-6 nm[Cr-1.1 nm/Fe-3 nm]×60/Cr-1.1 nm, (Ref. 15); 9—MgO/Fe(001)/Cr(001), (Ref. 14); 10—MgO/Cr(50 Å)/[Fe(100):3 ML+8 ML+3 ML/Cr(100)]$_{10}$, present work (sample 1); 11—MgO/Cr(50 Å)/[Fe(100): 0.7 ML+8 ML/Cr(100)], present work (average of samples 2–4); 12— MgO(100)/40 nm Cr/^{57}Fe(100)2 ML/^{56}Fe:2 nm/Cr:4 nm, (Ref. 10); GaAs(100)/Fe:1 nm/Ag 150 nm/^{56}Fe:4 nm/^{57}Fe(100): 2 ML/Cr:1 nm/^{56}Fe 4 nm; 13—magnetic moment calculations within PAM (present work) (lower abscissa)

$W(110)$ substrate.[12] Interpretation of CEMS spectra using the empirical approach Eq. (1) or Eq. (2) leads for the same set of hff to different conclusions about the local environment of ^{57}Fe atoms, their numbers of nearest (n_1) and next-nearest (n_2)Cr neighbors and, consequently, to the distinct spatial structure of the Fe/Cr interface region. The microscopic analysis of Fe/Cr interface magnetism, taking into account roughness and interdiffusion, then becomes very important for understanding the real physical information that can be extracted from CEMS data.

Most of the calculations of magnetic-moment distributions in intermixed Fe/Cr layers of multilayer systems were restricted to the ordered structure of the interface and to the very thin interface region, which include usually one to two monolayers. Coehoorn[19] performed the first-principal band-structure calculations for (110)- and (100)-oriented Fe/Cr superlattices with intermixed monolayers at the interfaces. He concludes that Fe and Cr moments at the Fe/Cr interface show almost no dependence on the nearest-neighbor environment. A change of the Fe concentration in the interface layer mainly affected the Fe moments in the Fe layer one atomic layer below the mixed layer. This is not very surprising,

because for a bcc lattice and for (100) interface orientation atoms do not contain nearest neighbors in the same layer, but only in the previous and next layers. The moments in the second and third layers below the mixed interface proved to be already quite independent of the concentration in the mixed layer, although they were found to be slightly above the calculated value for bulk ($2.26\mu_B$). Freyss *et al.*[20] modeled an interfacial alloy by either a one- or a two-monolayer-thick ordered compound whose concentration was varied. They performed self-consistent calculations within a tight-binding model Hamiltonian for a Cr overlayer on an Fe substrate, and showed that the more Cr and Fe interdiffused at the interface (inside two mixed layers), the more important is the decrease of the sample magnetization due to Cr coverage. All these approaches, which presuppose ordered interface layers instead of real rough interfaces, can give only a qualitative picture of the interference between magnetic and chemical structure. The role of interface chemical ordering as well as of the sensitivity of the calculated magnetic properties on this assumption needs special consideration.

The magnetic structure of disordered rough Fe/Cr interfaces was investigated on an atomic scale within the periodic Anderson model (PAM) in Ref. 21. Self-consistent calculations of magnetic moments were fulfilled for the set of rough interfaces modeled in the ballistic approach using the special algorithm ''epitaxy.'' This algorithm allows one to simulate random Fe/Cr multilayer structures with different, but controlled, alloying at the interface region. Magnetic characteristics of the Fe sample covered by thin Cr films, which were measured by different experimental methods, then can be modeled using an appropriate averaging procedure. In such a way the roughness-induced transition from the oscillation behavior to the exponential decrease of the total magnetic moment of the Fe sample with Cr coverage was described theoretically in Ref. 21. This transition takes place with increasing interface alloying, governed by the parameters of the epitaxy algorithm. An exponential decrease of the total moment was detected experimentally by Turtur and Bayreuther[3] using magnetometer measurements. In Ref. 22 a similar approach was used for the description of magnetic dichroism and spin-resolved photoemission data from rough interfaces. Together with the simplified theory for description of electron emission from rough surfaces, the calculated magnetic structure of a nonideal Cr/Fe overlayer gave reasonable agreement with experimental results by Knabben *et al.*[23]

In the present work we will use the same theoretical approach for the calculation of magnetic moments in Fe/Cr(001) superlattices with different types of interface roughness, and we investigate the correlation between the calculated magnetic structure and experimental hff distributions.

The paper is organized as follows. In Sec. II, the experimental procedure of sample preparation and CEMS measurements are described. In Sec. III we discuss the modeling of the interface roughness and interdiffusion by different random algorithms. In Sec. IV the results of self-consistent calculations for interfaces with different roughness are presented. In Sec. V we discuss the approach of Eqs. (1) and (2) for hff within the light of our calculations, and we compare magnetic-moment distributions for different rough interfaces with experimentally observed hff. Finally the paper is concluded in Sec. VI.

II. EXPERIMENTAL PROCEDURE AND RESULTS

Fe/Cr(001) superlattices were epitaxially grown by ultrahigh-vacuum deposition of the metals on epipolished MgO(001) substrates. The substrate surface was cleaned using isopropanol and (after insertion into the ultrahigh-vacuum system) heating at ~900 K for 1 h to remove surface contaminants and to anneal the surface. At a substrate temperature of ~900 K a 50-Å-thick Cr buffer layer was grown on MgO first. Preparing the buffer layer at this temperature gave the best results for epitaxial growth of Fe on Cr. Subsequently the Fe/Cr(001) superlattice was grown at 433 K at a pressure $<5\times10^{-9}$ mbar. This growth temperature provides good epitaxy and is below the growth temperature of ~500 K, where severe long-range Fe-Cr interdiffusion occurs.[9] High-purity materials (natural Fe: 99.9985 at. %, Cr: 99.999 at. %; ^{57}Fe: 95.5% and ^{56}Fe: 99.5% isotopically enriched) were evaporated from resistively heated Knudsen cells with deposition rates of 0.2–0.3 Å s^{-1}, as measured by calibrated quartz-crystal oscillators. We have investigated four types of samples of different composition:

$$\mathrm{MgO/Cr(50\,\text{Å})/[^{57}Fe(3\,ML)/^{nat}Fe(8\,ML)/^{57}Fe(3\,ML)/Cr(8\,ML)]\times10}\quad\text{(sample 1)}$$

$$\mathrm{MgO/Cr(50\,\text{Å})/[^{57}Fe(0.7\,ML)/^{nat}Fe(8\,ML)/Cr(8\,ML)]\times40}\quad\text{(sample 2)}$$

$$\mathrm{MgO/Cr(50\,\text{Å})[^{57}Fe(0.7\,ML)/^{nat}Fe(8\,ML)/Cr(8\,ML)]\times200}\quad\text{(sample 3)}$$

$$\mathrm{MgO/Cr(50\,\text{Å})/[^{57}Fe(0.7\,ML)/^{56}Fe(8\,ML)/Cr(8\,ML)]\times200}\quad\text{(sample 4)}.$$

In sample 1, 3-ML-thick ^{57}Fe probe layers were artificially placed at both types of interfaces (Fe deposited on Cr(=Fe/Cr, ''lower'' interface) *and* Cr deposited on Fe (=Cr/Fe, ''upper'' interface)). In samples 2–4, ultrathin 0.7-ML (1 Å)-thick ^{57}Fe probe layers were deposited at one type of interface only (''dusting'' of the Fe/Cr interfaces). The probe-layer method[24,25] provides an ^{57}Fe nuclear resonance (Mössbauer) signal predominantly from ^{57}Fe atoms in

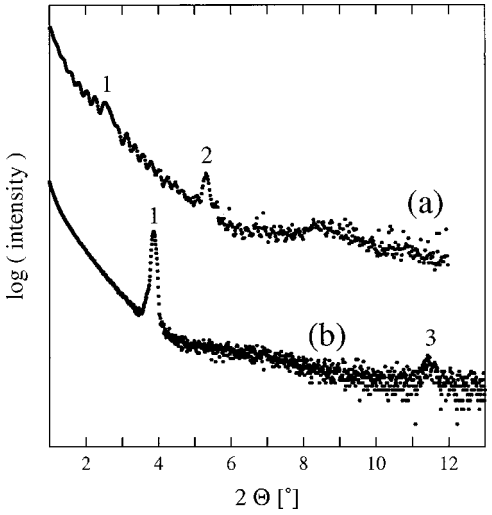

FIG. 2. Low-angle XRD intensity measured on (a) sample 1, (b) sample 3. The order of the Bragg diffraction peaks is marked by numbers. Note that the second-order peak is forbidden for sample 3 (Cu K_α radiation).

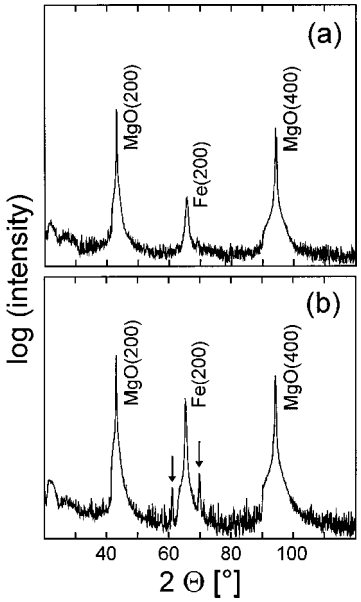

FIG. 3. High-angle XRD intensity measured on (a) sample 1, (b) sample 3. The arrows in (b) mark the first-order satellite peaks observed around the (200) Bragg peak of Fe. (Note that the second-order satellite peaks are forbidden for sample 3). The strong peaks near 43° and 93° belong to the (200) and (400) reflections, respectively, of the Mg(001) substrate (Cu K_α radiation).

the interface region in samples 1–3, and exclusively in the interface region in sample 4.

The multilayer structure of our samples was qualitatively characterized by conventional (θ–2θ) low-angle and high-angle diffraction (XRD). Representative XRD results are shown in Fig. 2 (low angle) and Fig. 3 (high angle) for sample 1 and sample 3. The samples with a low number of stacked Fe/Cr bilayers (e.g., like sample 1) generally exhibit first- and second-order low-angle superstructure Bragg peaks and intensity oscillations from total thickness interference [Fig. 1(a)]. Due to the large total thickness these oscillations disappear in samples with a high number of bilayers (like sample 3); but a strong first-order and weaker third-order low-angle superstructure peak is observed [Fig. 1(b)]. (Note that the second-order superstructure peak is forbidden for sample 3, because the individual Fe and Cr thicknesses are about equal.) These observations demonstrate that our samples have flat surfaces and good multilayer quality, which is preserved even up to a thickness of 200 bilayers (e.g., like sample 3). In high-angle XRD (Fig. 3), the (200) (and no other) Bragg reflection of bcc Fe was detected. The typical full width at half maximum (FWHM) of the rocking curve (not shown) of this peak was found to be about 2° for all samples. These results demonstrate the single-crystalline (epitaxial) nature of our samples. Typically two first-order satellite peaks [arrows in Fig. 3(b)] around the fundamental (200) reflection of bcc Fe were observed in samples with a large number of bilayers (e.g., like sample 3). (Again, the second-order satellite peaks are forbidden for sample 3). These observations provide a proof of the high superlattice quality of our samples up to 200 bilayers. However, for samples with a low number of bilayers (e.g., like sample 1) satellite peaks around (200) are difficult to detect, as expected [Fig. 3(a)]. According to magnetization hysteresis loops (not shown), the samples exhibit zero remanence, i.e., strong antiferromagnetic (AFM) interlayer coupling,[13] as expected for 8-ML Cr layers.

Mössbauer CEMS spectra were measured at room temperature (RT) using a He/CH_4-filled proportional counter and a ^{57}Co-in-Rh source. The incident γ radiation was perpendicular to the sample surface. Typical CEM spectra of samples 1–4 are shown in Fig. 4(a)–4(d), respectively. As compared to the simple Zeeman sextet of ferromagnetic bulk bcc Fe, the spectra in Fig. 4 exhibit distinct shoulders and extra peaks as a result of changes of the ^{57}Fe hff that are induced by neighboring Cr atoms in the interfacial ^{57}Fe-probe layers region.

The CEM spectra were least-squares fitted with two hff distributions ranging from 0 to 18 T (low-field region) and from 18 to 35 T (high-field region) for sample 1, and from 0 to 15 T (low-field region) and from 15 to 35 T (high-field region) for samples 2–4. For the fitting, the NORMOS computer program by Brand[26] was used, which is based on the histogram method by Hesse and Rübartsch.[27] In order to achieve satisfying fitting, a linear correlation between hff and isomer shift had to be assumed, and, further, the line-intensity ratios of the basic sextets in the hff distributions were supposed to be 3:4:1, implying Fe-spin orientation in the film plane.

The hff distributions, $P(B_{\rm hf})$, are shown in Fig. 5. The high-field distributions of all samples exhibit six pronounced maxima, located at $B_{\rm hf}=33.1$, 30.6, 28.0, 25.2, 22.7, and 19.6 T, respectively, for sample 1, and at $B_{\rm hf}=33.2$, 30.3, 27.9, 25.0, 22.6, and 19.7 T for samples 2–4 (averaged). An additional peak at 16.9 T is observable in Fig. 5 for samples 2–4 only, which have a smaller average probe-layer thickness (0.7-ML ^{57}Fe) than sample 1 (3-ML ^{57}Fe). The observed hff value of 33.2 T is equal to the bcc-Fe bulk value, $B_{\rm hf}$ (bulk), at 300 K, and evidently is associated with ^{57}Fe

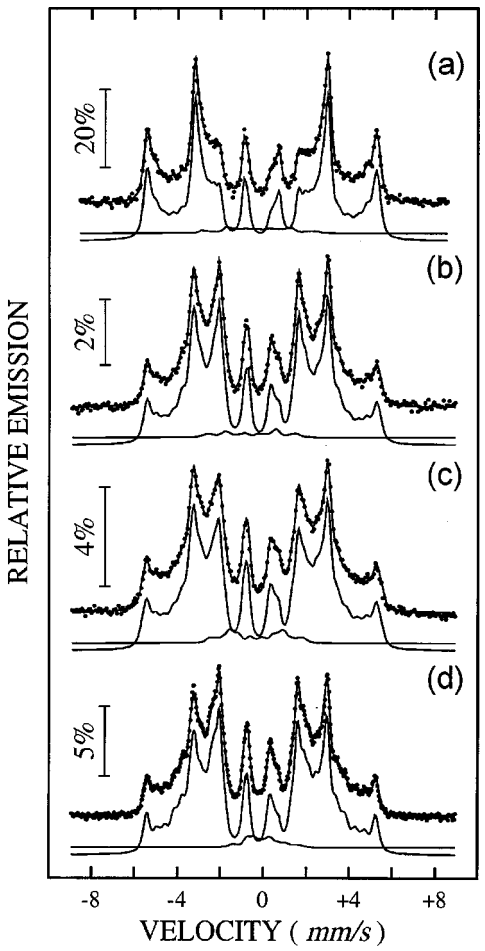

FIG. 4. CEM spectra of Fe/Cr(001) superlattices, measured at 300 K: (a) sample 1: [^{57}Fe(3 ML)/^{nat}Fe(8 ML)/^{57}Fe(3 ML)/Cr(8 ML)]×10; (b) sample 2: [^{57}Fe(0.7 ML)/^{nat}Fe(8 ML)/Cr(8 ML)]×40; (c) sample 3: [^{57}Fe(0.7 ML)/^{nat}Fe(8 ML)/Cr(8 ML)]×200; (d) sample 4: [^{57}Fe(0.7 ML)/^{56}Fe(8 ML)/Cr(8 ML)]×200. Full-drawn curves: result of least-squares fit with distribution of hyperfine fields, $P(B_{hf})$.

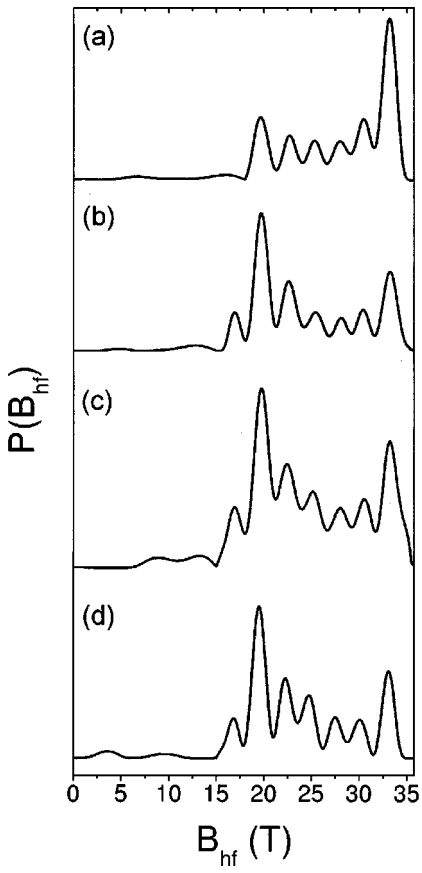

FIG. 5. Hyperfine-field distribution, $P(B_{hf})$, obtained from Fig. 4: (a) sample 1, (b) sample 2, (c) sample 3, and (d) sample 4.

atoms in a ''bulklike'' environment without nearest ($n_1=0$) or next-nearest ($n_2=0$)Cr neighbors. Note in Fig. 5 that the relative intensity (relative area) of this bulk peak is remarkably higher for sample 1 (40%) than for samples 2, 3, and 4 (19, 19.5, and 15.9%, respectively), as is expected regarding the larger probe-layer thickness (3-ML ^{57}Fe) of sample 1, and assuming the same degree of slight and unavoidable intermixing of ^{56}Fe and ^{57}Fe on an atomic scale of 1 to 2 ML[9,10] in all types of samples. The weakest 33-T peak (relative area 15.9%) is observed in the distribution of sample 4 [Fig. 5(a)], because ^{57}Fe does not exist in the central part of the ^{56}Fe films. Conversely, one should notice in Fig. 5 the strikingly higher relative intensity of the hff distribution peak at 19.7 T for samples 2–4, as compared to sample 1. Since only the relative intensity of the individual hff distribution peaks (or of the individual subspectra) is modified by changing the ^{57}Fe-probe-layer thickness, and *not* their individual positions, each $P(B_{hf})$ peak originates from a certain characteristic ^{57}Fe environment (site) within the Fe-Cr interfacial region. For instance, according to the model by Landes *et al.*,[9] the experimental hff of 20.9 T (which is close to our 19.7-T value) was attributed to the ideal (flat) interface site, while Schad *et al.*[14] assigned a value of 19 T for this site. In a refined analysis Klinkhammer *et al.*[10] reported a value of 23.0 T for the ideal (flat) interface site ($n_1=4$, $n_2=1$ or (4/1) site).

It is remarkable in Fig. 5 that the low-field $P(B_{hf})$ distributions contribute only very little (about 3% or less) to the total area of the hff distribution (or to the total area of the Mössbauer spectra). In particular, there is a neglible contribution near $B_{hf}\approx 0$ T of a paramagnetic subspectrum for our samples, such as it arises for paramagnetic isolated Fe atoms in a bulk Cr matrix.

In Fig. 1 we compare the hff values at the observed maxima in $P(B_{hf})$ of our samples with corresponding results reported in the literature (top abscissa in Fig. 1). Obviously, there is reasonable agreement regarding certain hff values in our samples, in molecular beam epitaxy (MBE)-grown[9,10,14] and sputtered samples,[15] and even in MBE-grown samples with (110) orientation.[12] Not included in Fig. 1 are hff distribution peaks of sputtered Fe/Cr superlattices on MgO(001) that were observed[16] at $B_{hf}=33.3$, 30.7, 26, 22, 20, and 10 T and are negligible near zero-hff (paramagnetic) contributions (at $B_{hf}<\sim 1.0$ T), similar to our case. We like to emphasize again that the enhanced (larger than bulk) B_{hf} value, which appears to be characteristic of the second Fe layer below the ideally flat Fe/Cr interface, has been convincingly detected

only in molecular-beam grown epitaxial Fe/Cr systems with relatively smooth interfaces.[9,10,12] The enhanced hff was observed neither in our UHV-deposited superlattices, nor in sputtered Fe/Cr systems,[11,15,16] very likely due to a larger interface roughness as compared to MBE-grown structures.

III. MODELING OF THE ROUGH INTERFACES

The evolution of a growing interface is a very complicated phenomenon that depends on the internal interactions between atoms as well as on the number of external factors.[28] For the Fe/Cr systems, where both elements have almost the same lattice constant, alloying processes cannot be completely avoided. Epitaxial growth leads to an interface structure that, as a first approach, can be considered as a superposition of steps and an alloy with varying concentration. It is also important that the process of alloying may be substantially nonsymmetric: this is essential, when the substrate material has a lower melting temperature than the adatom material.[2,8] This will be the case for evaporating Cr on Fe, but for Fe on Cr alloying should be suppressed. However, for the rough Cr surface alloying after Fe deposition also can occur. The scenario of alloying as well as the result of this process at different interfaces in Fe/Cr multilayers can be essentially different.

For the investigation of the magnetic-moment distribution near the rough Fe/Cr interface, and for further comparison of it with the distribution of hff obtained from the CEM spectra, we developed several random algorithms that allow one to create the superlattices with different types of interface roughness. The period of all superlattices was taken equal to 22 monolayers: 8-ML Cr and 14-ML Fe, in order to obtain the structures, similar to the ones studied in the experiment (Sec. II). We also used different kinds of Fe atoms (sites) for comparison with Mössbauer results, when only hff at the ^{57}Fe nuclei are measured. Taking into account that in our experiments we used about 1- and 3-ML-thick ^{57}Fe-probe layers in the interface region, for the modeling of such a system we create superlattices with period Fe1(1 ML)/Fe2(2 ML)/Fe3(8 ML)/Fe2(2 ML)/Fe4(1 ML)/Cr(8 ML). Here, through the label Fe1, Fe2, etc., we denote the different kinds of Fe atoms within an individual Fe layer of the Fe/Cr multilayer. All of these Fe atoms are fully identical and have the same set of parameters in the model Hamiltonian, but the distribution of magnetic moments can be obtained not only on all the Fe and the Cr atoms, but also separately on the Fe atoms of a given type. For example, for comparison of the hff distribution measured for the superlattice with 3-ML ^{57}Fe at every ''Fe/Cr'' and ''Cr/Fe'' interface with the calculated distribution of the magnetic moments, we have to find the magnetic moments localized on Fe1, Fe2, and Fe4 sites, whereas for a superlattice with only 1-ML ^{57}Fe at the Cr/Fe interface we need the magnetic moments of Fe4 atoms.

Interface roughness was introduced into the model by two kinds of random procedures: the first one produces atomic steps at the interface, whereas the second one models interface alloying and interdiffusion. For modeling of the stepped interfaces we started from the ideal superlattice, where all the layers contain only Cr or Fe atoms. In the plane we used a

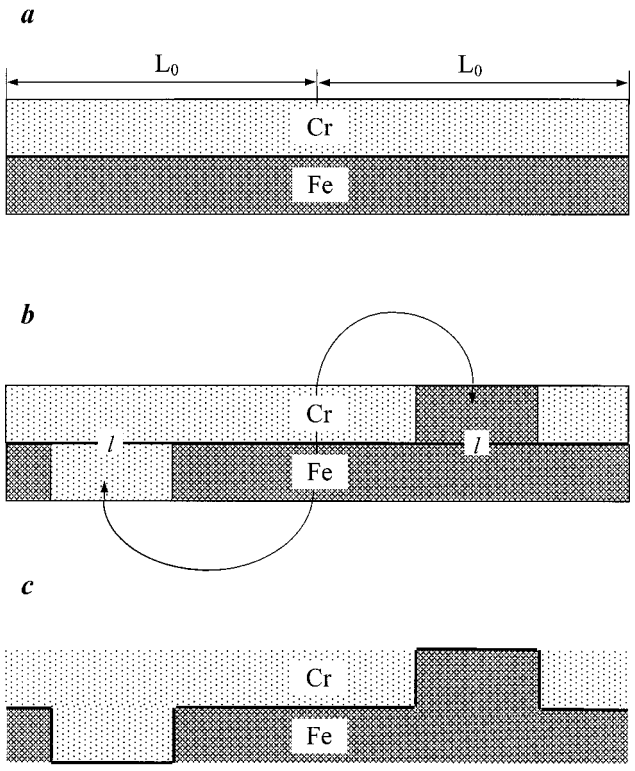

FIG. 6. Modeling of stepped interface.

64×1 cell with periodic boundary conditions. The total length of the cell (64 sites) was divided into an even number of equal intervals L_0 [Fig. 6(a)], where L_0 is the parameter of the algorithm. Then, for every pair of neighboring intervals a random number $l<L_0$ was chosen, and l successive interface Fe atoms from the first interval have been exchanged with l successive interface Cr atoms from the second interval [Fig. 6(b)]. The position of l atoms inside the interval L_0 was taken as random. As a result we obtained the stepped interface where one-ML high upsteps alternate with one-ML high downsteps, and the lateral size of every step does not exceed L_0 [Fig. 6(c)]. Obviously only atoms Fe1 and Fe4 can be in the mixed Fe/Cr layers. Decreasing the parameter L_0 leads to the formation of interfaces with larger density of steps per unit of length. In the direction perpendicular to the plane direction the system stays spatially homogenous. Modeling of every superlattice was repeated 20 times to obtain the distributions that do not depend on concrete realization.

Alloying and interdiffusion have been simulated in the ballistic regime using the algorithm epitaxy.[21,22] This algorithm fills the prism with cross section 8×8 atomic sites by Fe and Cr atoms. Outside the prism the structure was repeated periodically. The height of the prism was taken as 30 layers, but only 22 layers were cut for self-consistent calculations of magnetic moments to reproduce the superlattice structure with period 22 ML. Initially, the bottom layer of the prism was filled by Fe3 atoms, and all the other sites inside the prism were empty. Then new atoms are thrown on the top level of the prism with a random procedure, and the epitaxy routine provided their descending through empty sites in the bcc lattice until the sliding is blocked. Transfer of

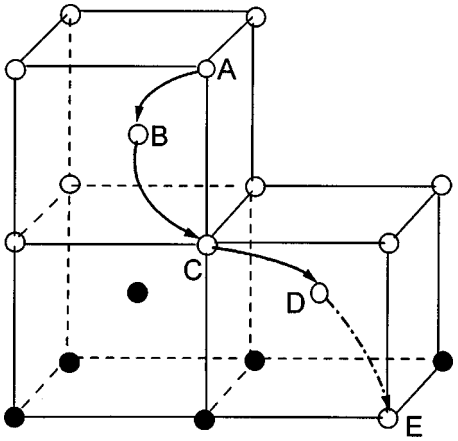

FIG. 7. Modeling of alloying using the epitaxy algorithm.

atoms from one layer to the next layer occurs with equal probability to any of the nearest-neighbor sites. If we put on the top of the prism $64\times N_{\mathrm{Fe}}$ atoms of Fe and after that $64\times N_{\mathrm{Cr}}$ atoms of Cr we will obtain the structure $\mathrm{Cr}(N_{\mathrm{Cr}})/\mathrm{Fe}(N_{\mathrm{Fe}})$ with a rough interface. Taking into account that the surface layer is not fully filled by the atoms, we throw away a few top and bottom layers and put periodic boundary conditions for the remaining layers in the prism. In such a way we obtain a Fe/Cr superlattice with rough Fe/Cr and Cr/Fe interfaces. Every such modeling was repeated 20 times, like in the case of the stepped interface.

Figure 7 shows the random walk of the atom in the bcc lattice. Empty circles depict sites that are not filled by atoms. The atom stops its movement, if all four possible next positions are blocked. If only part of these four position is blocked, the atom may either continue its descent with probabilities p_i through each empty site or it may stop at a particular site with the probability $1-\Sigma_i p_i$. The quantities p_i have been taken to depend on the amount of blocked path. The set of p_i values is the input parameter of the epitaxy algorithm. Different p_i values lead to distinct surface and interface structures. In our modeling we used two sets of p_i:

(A) $p_i=1/n$, where n is the number of empty nearest-neighbor sites in the next layer. In this case the atom is forced to move, if at least one of the nearest sites in the next layer is empty. Surfaces and interfaces generated by the algorithm epitaxy turn out to be relatively smooth. The width of the interface region, where there are both Fe and Cr atoms, does not exceed 3 to 4 ML, and the sample does not contain any empty sites in inner layers. We will identify such an interface as ''smooth.''

(B) $p_i=1/4$ for $n=1$ and for $n=2$; $p_i=1/3$ for $n=3$. Here, the atom can stop its descent, if there are only one or two available sites in the next layer. The interface structure proves to be more irregular with some hollow sites and interface mixing of Fe and Cr atoms in a 7- to 10-ML-thick region.

To simulate interface intermixing of Fe and Cr atoms we used the *B* variant for Fe-on-Fe and Cr-on-Cr growth and the *A* variant for growth Fe on Cr and Cr on Fe. However, even so, some empty sites remained in the inner layers. To remove these pores inside the sample we filled empty places by Cr and Fe atoms using two different procedures: (i) on an empty place we put Fe, if most of the nearest-neighbor sites are filled by Fe, and in the opposite case this place was filled by Cr; (ii) all the empty sites were filled by Fe atoms. For procedure (i) additional Fe atoms cannot appear inside the Cr spacer. The concentration of Fe in Cr and Cr in Fe decreases toward zero away from the interface. Due to the relatively thick interface region we will call such an interface as ''rough.'' Procedure (ii) gives the structure with a constant, although relatively small, Fe concentration far enough from the interface. In the following such a structure will be denoted as ''rough+alloy.''

Note that our epitaxy algorithm corresponds to the ''ballistic deposition'' in the theory of epitaxial growth.[29] Variants *A* and *B* of the algorithm move or stop atoms depending on the number of bonds with its nearest neighbors that the deposited atom has. This can be considered as a simplified ''bond counting'' approach.

The distribution of Fe atoms, which have given numbers of Cr nearest (n_1) and next-nearest (n_2) neighbors, is presented in Table I for different kinds of rough interfaces. The left column in the table specifies the local environment of Fe atoms, n_1/n_2. For every structure we depicted the numbers for the whole Fe atoms (I), for the Fe atoms from the 3-ML-thick interfacial layers at every Fe/Cr and Cr/Fe interface: Fe(1)+Fe(2)+Fe(4) (II), and for 1 ML at the Fe/Cr interface: Fe(4) (III). Note that for the structure ''rough+alloy'' additional Fe atoms, which appear inside the Cr spacer, instead of empty places were taken as Fe(4), and inside Fe layers as Fe(3).

Simple analysis of the data in Table I shows that the fraction of Fe atoms with a given local environment is strongly connected with the type of interface roughness. Stepped interfaces contain only Fe atoms in 0/0, 0/1, 2/1, 2/2, 4/1, 4/2, and 4/3 configurations, and all Fe atoms that have Cr neighbors lie in the 3-ML-thick interface layers. Among atoms from first interface layers there are no bulklike atoms (0/0). It means that for such stepped structures with 1-ML ^{57}Fe at the interface the bulk contribution to the hff has to be almost fully suppressed. Comparison of the distributions for 1- and 3-ML-thick interface layers demonstrates that, depending on the size of the steps, different configurations become more or less probable. In particular, for $L_0=16$ one can find Fe atoms in the 4/1 state much more often than in the 4/2 state. For $L_0=4$, the corresponding ratio among these Fe sites from the 3-ML-thick interface is not far from unity, and it becomes less then unity for the atoms in the 1-ML-thick interface.

The structure with interface alloying is characterized by a wider atomic distribution between states with different local environments. This distribution expands with increasing roughness due to Fe atoms that penetrate deeper into the Cr spacer and fill the states with a large number of Cr neighbors. Whereas for the ''smooth'' interface only Fe atoms with $n_1\leqslant 4$ are present, for the rougher structures there are states with all possible numbers of Cr nearest neighbors up to eight. The number of nearest neighbor Cr atoms n_1 and next-nearest neighbors n_2 is also correlated for the rough structure under investigation. For every n_1 there is n_2^*, which corresponds to the most probable configuration with a

TABLE I. Simulated distribution of Fe atoms that have given number of nearest (n_1) and next-nearest (n_2) Cr neighbors for different kinds of rough interfaces. Left column: local environment of Fe atoms, labeled n_1/n_2. For every structure (stepped, smooth, rough, or rough+alloy interface) the numbers for all of the Fe atoms (I), for Fe atoms from 3-ML-thick layers at every Fe/Cr and Cr/Fe interface [Fe(1)+Fe(4)](II), and for 1 ML at the Cr/Fe interface [Fe(4)](III) are depicted.

	Stepped $L_0=16$			Stepped $L_0=4$			Smooth			Rough			Rough+alloy		
Config.	I	II	III	I	II	III	I	II	III	I	II	III	I	II	III
0/0	19195	3835	0	19224	3864	0	19 200	3915	17	13 908	4064	90	14035	4139	97
0/1	3600	3600	489	2911	2911	386	2197	2123	95	1569	1078	95	1625	1108	109
0/2	0	0	0	0	0	0	0	0	0	75	56	0	144	102	1
1/0	0	0	0	0	0	0	0	0	0	986	599	72	1226	771	99
1/1	0	0	0	0	0	0	1169	1168	145	1461	1128	188	1415	1075	198
1/2	0	0	0	0	0	0	0	0	0	364	283	44	423	304	58
1/3	0	0	0	0	0	0	0	0	0	48	37	4	87	58	7
2/0	0	0	0	0	0	0	0	0	0	145	103	21	267	207	56
2/1	431	431	91	1427	1427	239	863	863	196	835	658	220	847	679	239
2/2	49	49	29	431	431	241	74	74	20	615	480	145	616	466	159
2/3	0	0	0	0	0	0	0	0	0	203	152	36	249	158	46
2/4	0	0	0	0	0	0	0	0	0	24	17	5	64	42	16
3/0	0	0	0	0	0	0	0	0	0	3	1	1	64	50	12
3/1	0	0	0	0	0	0	824	824	295	400	317	108	437	355	129
3/2	0	0	0	0	0	0	317	317	119	601	462	159	541	434	174
3/3	0	0	0	0	0	0	50	50	24	397	300	93	421	325	137
3/4	0	0	0	0	0	0	0	0	0	108	76	24	200	128	57
3/5	0	0	0	0	0	0	0	0	0	8	7	3	46	23	16
4/1	3177	3177	1098	1592	1592	462	662	662	295	71	56	16	103	93	27
4/2	415	415	207	1211	1211	607	658	658	295	276	223	75	293	259	133
4/3	8	8	2	108	108	47	400	400	194	407	336	113	415	362	220
4/4	0	0	0	0	0	0	303	303	147	283	225	74	323	280	197
4/5	0	0	0	0	0	0	163	163	78	69	55	21	166	146	126
4/6	0	0	0	0	0	0	0	0	0	0	0	0	22	18	18
5/1	0	0	0	0	0	0	0	0	0	4	4	0	24	24	11
5/2	0	0	0	0	0	0	0	0	0	37	36	11	90	89	56
5/3	0	0	0	0	0	0	0	0	0	154	136	50	266	265	197
5/4	0	0	0	0	0	0	0	0	0	220	197	82	333	333	288
5/5	0	0	0	0	0	0	0	0	0	106	88	40	285	285	267
5/6	0	0	0	0	0	0	0	0	0	7	6	1	82	80	80
6/3	0	0	0	0	0	0	0	0	0	14	13	4	92	92	79
6/4	0	0	0	0	0	0	0	0	0	67	65	25	262	262	246
6/5	0	0	0	0	0	0	0	0	0	82	80	40	340	340	333
6/6	0	0	0	0	0	0	0	0	0	11	11	5	196	196	195
7/3	0	0	0	0	0	0	0	0	0	0	0	0	26	26	25
7/4	0	0	0	0	0	0	0	0	0	7	7	5	124	124	123
7/5	0	0	0	0	0	0	0	0	0	22	22	19	250	250	250
7/6	0	0	0	0	0	0	0	0	0	14	12	10	208	207	204
8/4	0	0	0	0	0	0	0	0	0	1	1	1	28	28	28
8/5	0	0	0	0	0	0	0	0	0	6	6	4	79	79	79
8/6	0	0	0	0	0	0	0	0	0	24	22	16	99	99	99

given n_1. With increasing n_1 the value n_2^* also monotonously increases. Among the atoms within 1 ML at the interface the state without neighboring Cr atoms (0/0) for the alloyed interfaces is also suppressed, but not fully like in the case of stepped structures.

IV. DISTRIBUTION OF MAGNETIC MOMENTS FOR INTERFACES WITH DIFFERENT ROUGHNESS

Calculations of the magnetic moment distribution were performed within the PAM in Hartree-Fock approximation by the real-space recursion method.[21,30] For numerical calcu-

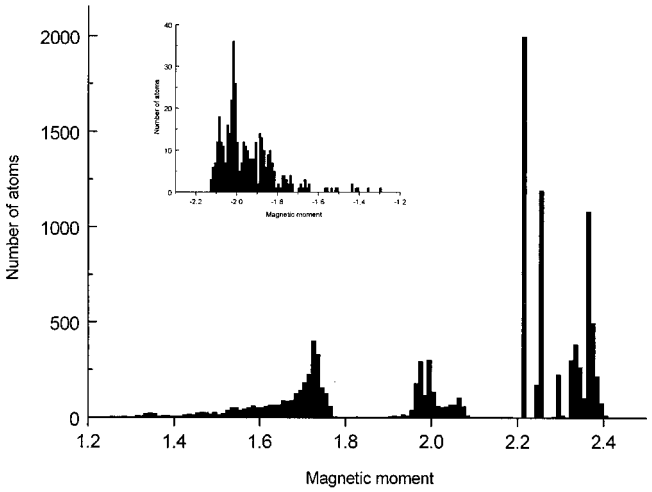

FIG. 8. Calculated distribution of magnetic moments (in μ_B) in the 3-ML-thick interface layers for the stepped interface with $L_0 = 4$. The inset shows the distribution of moments for the Fe atoms with opposite direction of magnetization (antiparallel to the overall magnetization direction).

lations we used the modification of the ''zero and poles'' method, which allows to determine very effectively the poles of the mass operator and the Green function, and to avoid time-consuming numerical integration of density of *d*-electron states in the process of self-consistency.[31,32] The self-consistency procedure starts from the state where all magnitudes of the magnetic moments on Fe and Cr sites were equal to the corresponding bulk values and the direction of the moments on Fe sites were taken to coincide, whereas on Cr sites both spin polarizations were available with equal probability. Calculations of magnetic moments were performed to obtain self-consistency both on every site and between magnetic moments localized on different sites. One more procedure fitted the Fermi energy, which fixes the total number of *d* electrons during self-consistency.

For both stepped interfaces (with $L_0=4$ and $L_0=16$) we obtain very similar distributions of magnetic moments, where deviation from the bulk value takes place only inside 3-ML-thick interface layers. In Fig. 8 such a distribution is shown for $L_0=4$. The distribution function contains few sharp maxima, one of which corresponds to the bulk moment, and others to the enhanced moment up to $2.40\mu_B$. There are two extended maxima with less amplitude in the region $1.5-1.8\mu_B$ and $1.95-2.05\mu_B$. The shape of the distribution function is essentially asymmetrical near these maxima. In the neighborhood of the first maximum it slowly increases from 1.5 to $1.75\mu_B$, and then drops to zero very fast. Around the second maximum it has a longer tail from the side of larger moments. There are also some Fe atoms that change the direction of magnetization under the action of Cr neighbors. Their moment distribution is shown in the inset of the Fig. 8. Fe atoms from the 1-ML-thick interface layer show really full suppression of the bulk moment in accordance with data in Table I.

As a check of the assumption about the additivity of the Fe-magnetic moment perturbation by nearest neighbor and next-nearest neighbor Cr atoms we plotted the distribution of magnetic moments among the atoms that have a given number of Cr neighbors. Analysis of these dependencies for the stepped interface shows that enhancement of the magnetic moments takes place mainly for Fe atoms in the 0/1 state. Note that similar enhancement of magnetic moments for the Fe atoms inside clusters and pinhole defects embedded into the Cr matrix was observed in Refs. 30, 33, and 34. This moment enhancement is correlated with hff data,[9,10,12] where for the second Fe layer below the ideal interface an enlarged hff was assumed [see Eq. (2)]. There is, however, also a very small amount of Fe atoms in the same 0/1 state, which has a small moment of about $1.5-1.6\mu_B$. A clearer separation in low- and high-spin states can be seen, for example, for the Fe atoms with two Cr nearest and one next-nearest neighbors [Fig. 9(a) and 9(b)]. The low-spin state has the moment $1.70-1.78\mu_B$ for 2/1 configuration (and $1.65-1.75\mu_B$ for 2/2 configuration, not shown). Correspondingly, high-spin moments lie in the regions $1.95-2.10\mu_B$ [Fig. 9(a) and 9(b)] and $1.98-2.05\mu_B$ (not shown). Among the Fe atoms at the interface that have four nearest-neighbor Cr atoms we found a noticeable part that changes the direction of their moments opposite to the direction of the average magnetization.

In general, there is the tendency for a decrease of the moments by increasing the number of Cr neighbors. However, the existence of two different magnetic states with essentially different moments for the same number of Cr neighbors does not allow to conclude on an additive influence of the Cr neighbors. Similar results concerning nonadditive perturbation of Fe magnetic moments were obtained in Ref. 35 for the dilute FeCr alloy, and were explained by the sensitivity of Cr magnetic moments to the local environment. The Cr moments for the stepped interface have a very wide distribution with moments ranging from 0 to $1.2\mu_B$ [Fig. 10(a)]. Such a behavior is caused by frustration effects that appear due to Fe-Cr and Cr-Cr antiferromagnetic (AF) coupling. The ground state in the superlattices with stepped interfaces corresponds to the noncollinear ordering.[36]

Alloying and interdiffusion at the interface lead to a distribution of the magnetic moments that contains a larger number of maxima, although some of them confluence with increasing roughness. Figures 11(a) and 11(b) show such distributions corresponding to 3-ML-thick layers at both interfaces and to 1-ML-thick layers at the Fe/Cr interfaces, both for the case of a ''smooth'' structure. The distribution functions contain well-separated maxima, which give the most probable values of the Fe moments. The largest maximum (1690 atoms in the 3-ML-thick interface with a moment of $2.20-2.21\mu_B$) corresponds to the bulk Fe moments. For the 1-ML-thick layer at the Fe/Cr interface this peak becomes much lower, which reflects the reduction of the number of Fe atoms in the 0/0 state for 1 ML at the interface (see Table I). In both figures, 11(a) and 11(b), there is a peak for the enhanced magnetic moment of order $2.35\mu_B$. For 1 ML at the interface this peak is well separated from the bulk peak by a gap [Fig. 11(b)], but for 3-ML-thick interface layers the gap disappears [Fig. 11(a)]. Other maxima correspond to lower-than-bulk moments: around $2.0\mu_B$, $1.85\mu_B$, and in the region $1.6-1.7\mu_B$. These intervals, where the distribution

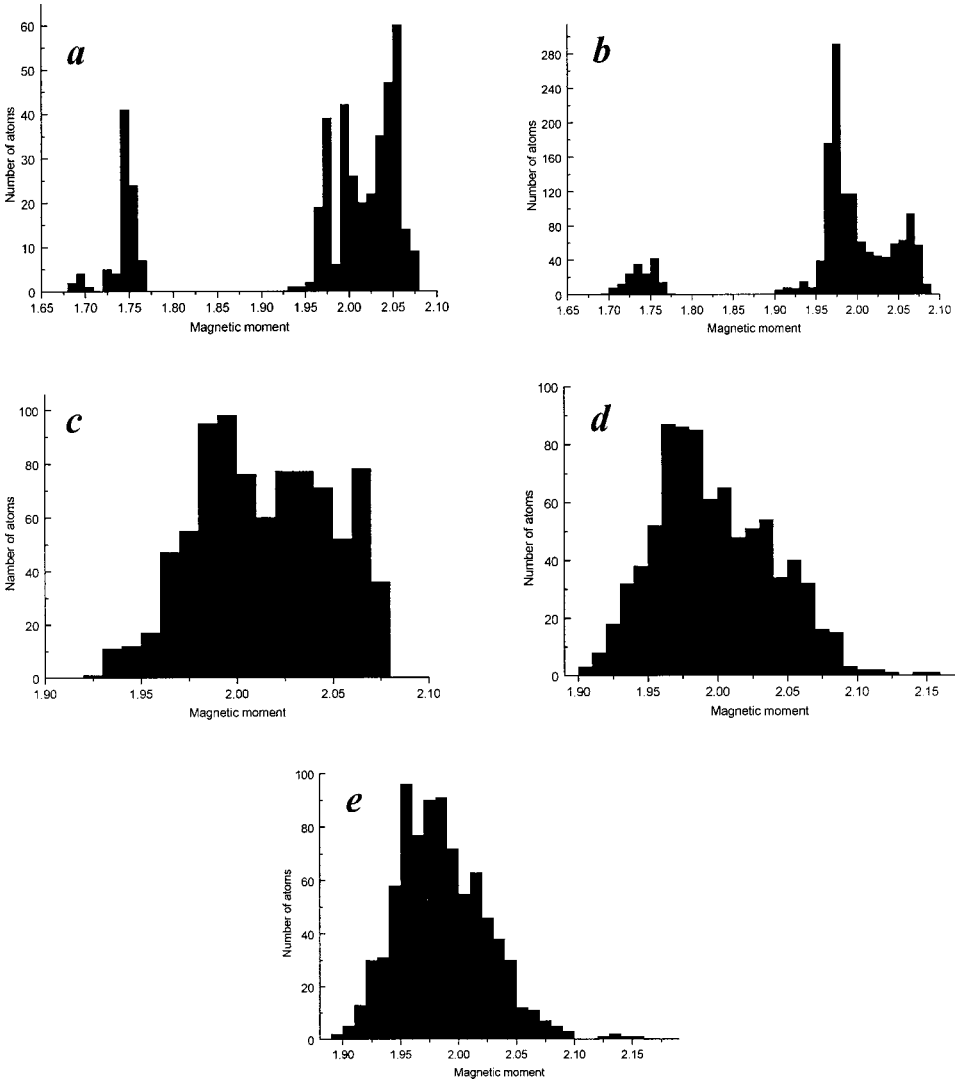

FIG. 9. Calculated distribution of magnetic moments (in μ_B) of (2/1) Fe atoms with two Cr nearest neighbors and one Cr second-nearest neighbor: (a) and (b) for the stepped interface with $L_0=16$ and $L_0=4$, respectively. (c)–(e) for the interfaces with interdiffusion: (c) smooth (d) rough, (e) rough+alloy.

function has its maxima, are shown also in Fig. 1 for comparison with hyperfine fields measured by CEMS. One can see a strong correlation between distribution peaks of hff and magnetic moments. However, calculated peaks for magnetic moments lower than $1.5\mu_B$ cannot be reproduced for the smooth interface. The moment distribution for Fe atoms with a given number of nearest-neighbor and next-nearest neighbor Cr atoms shows a relatively complex fine structure. For the Fe atoms in the 2/1 state [Fig. 9(c)] there is no separation of low- and high-spin states with a large difference in the moments, but the magnetic moments lie in the interval $1.95-2.08\mu_B$ (without deep well-pronounced minima inside this interval). States with a larger number of neighboring Cr atoms typically have a distribution function with several maxima (2/2, 3/2, 3/3, 4/3, 4/4, 4/5 states), but the distance between these maxima does not exceed $0.2\mu_B$. At the same time, every configuration is characterized by the interval of possible values of magnetic moments, and for some configurations these intervals do not overlap. For example, Fe atoms in 0/1 configuration have moments between 2.25 and $2.41\mu_B$, whereas for atoms in 1/1 configuration the moments lie in the interval $2.11-2.25\mu_B$. Fe atoms with two, three, and four nearest Cr neighbors have moments in the intervals $1.93-2.08\mu_B$; $1.70-1.90\mu_B$, and $1.3-1.7\mu_B$, respectively. Such a separation of the possible values of magnetic moments for every local environment does not mean additive perturbation of the Fe moments by Cr atoms. For rougher interfaces the peak positions of the distribution function do not change essentially. Figure 12 shows the moment distribution for a 3-ML-thick interface in the case of the rough [Fig. 12(a)] and the rough+alloy [Fig. 12(b)] structure. Now the state with the enhanced moment cannot be separated from the main peak corresponding to the bulk moments. Taking into account the large amplitude of the bulk peak and its close position to the nearest peak from the left side (about $2.15\mu_B$), one can conclude that only an increase of the half-width of the bulk maximum, but not its fine structure, will be possible to observe experimentally. The next maxima at $2\mu_B$, $1.85\mu_B$, and near $1.7\mu_B$ change their position only slightly with increasing roughness. For rough interfaces with alloying, we found some Fe atoms, as a rule, with a large number of Cr neighbors that change their magnetic moment direction opposite to the overall magnetization direction. The distribution of moments for such Fe atoms is shown in the inset of Fig. 12(b). It is a Gaussian-like distribution centered at $-1.5\mu_B$ with a half-width of about $0.3\mu_B$. Fe atoms re-

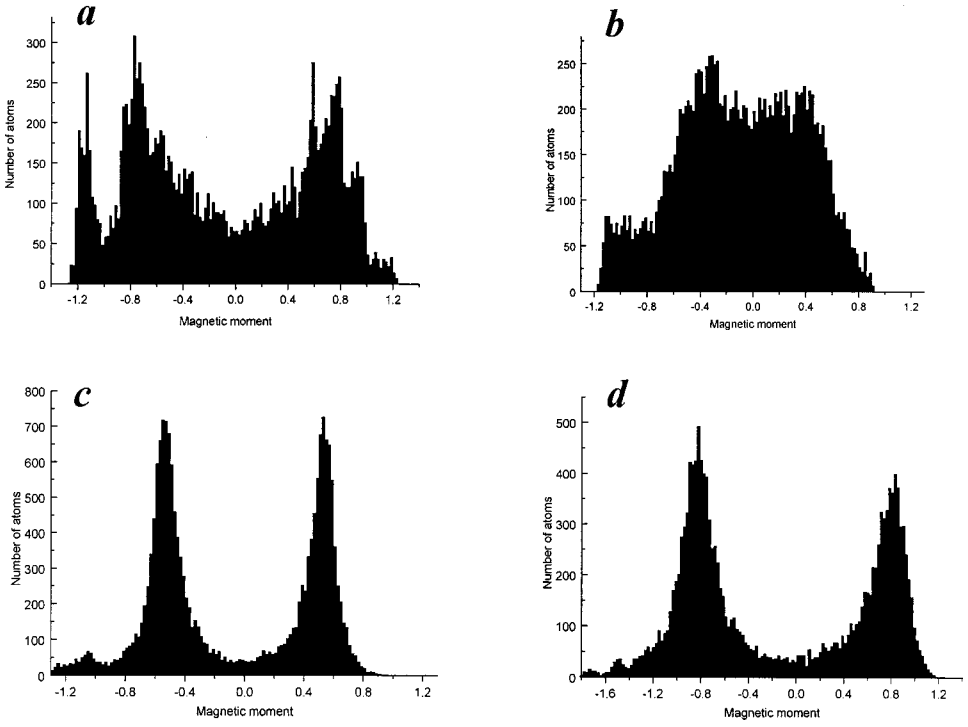

FIG. 10. Calculated distribution of magnetic moments (in μ_B) of Cr atoms for the superlattice with different interface roughness: (a) stepped interface with $L_0=4$; (b)–(d) interfaces with interdiffusion: (b) smooth, (c) rough, and (d) rough+alloy.

sponsible for this peak have five and more Cr nearest neighbors. The corresponding hff value was detected in some CEMS experiments, where the interface was not very smooth. In Fig. 1 the value of the moment ($1.5\mu_B$) for such Fe atoms is shown by a hatched square.

For the rough interface we obtain also the peak near $1.4\mu_B$. However, for other roughnesses it is not seen, because small Fe moments strongly depend on the states of the surrounding atoms and give a very wide distribution without distinct peaks. Maybe including some correlations in the algorithm of growth will lead to preferred configurations and to the formation of peaks, as compared to an almost constant distribution of moments.

The intervals of possible values of the magnetic moments for Fe atoms with given numbers of nearest and next-nearest Cr neighbors almost do not change with increasing roughness, as is seen in Figs. 9(c)–(e), although the fine structure of the distribution function is gradually washed out. In random alloys there is a correspondence between the perturbation of Fe magnetic moments and the numbers of nearest and next-nearest Cr neighbors in the average, but on an atomic scale such mapping fails.

Very sensitive to the interface roughness proves to be the distribution of the moments on Cr atoms. At the beginning of the self-consistency procedure the directions of the moments at the Cr sites were chosen ''up'' and ''down'' with equal probability. However, self-consistency leads to the AF structure, when Cr moments change their direction from layer to layer. For the smooth interface, significant intermixing of the Fe and Cr atoms takes place only in two interface layers. Frustration, which is determined by the tendency of Cr to AF coupling with Fe as well as with Cr neighbors, leads to the strong suppression of the moment, as is seen in Fig. 10(b). Increasing roughness and penetration of Fe atoms into the Cr spacer and Cr atoms into the Fe layer over a distance of several ML from the interface give a more regular distribution of the moments with two sharp peaks around $\pm 0.55\mu_B$. The appearance of additional Fe atoms inside of the Cr spacer far from the interface leads to additional polarization of Cr moments. The layered AF structure remains unchanged, however, and Fe atoms surrounded mainly by Cr atoms acquire the direction of the moments like Cr in the same layer. The presence of the Fe atoms surrounded by relatively large Cr magnetic moments induces an increase of the average Cr moments from 0.55 to $0.8\mu_B$ [Fig. 10(d)]. An additional peak in the distribution function for Cr moments at large negative moments (near $-1.1\mu_B$) appears due to Cr atoms at the interface with a large number of Fe neighbors. This peak is stronger for the stepped interface and decreases with increasing intermixing of Fe and Cr atoms.

V. DISCUSSION

The calculated distributions of magnetic moments for Fe/Cr superlattices including interface alloying and interdiffusion show a strong correlation with distributions of hff measured by CEMS. We found that both the position of satellite peaks in the CEM spectra and the position of maxima in the distribution function for local magnetic moments are stable relative to changes in the alloylike interface roughness. The observed correlation allows to say that in Fe/Cr layered structures the localized magnetic-moment scales with the hff on ^{57}Fe nuclei in a similar way as for bulk materials.[17,37] This is at variance with calculations according to the embedded cluster model for bulk Fe/Cr alloys,[38] where the proportionality between hff and local magnetic moments was not found. However, our findings for the moments are in good agreement with results of *ab initio* calculations[19] and of

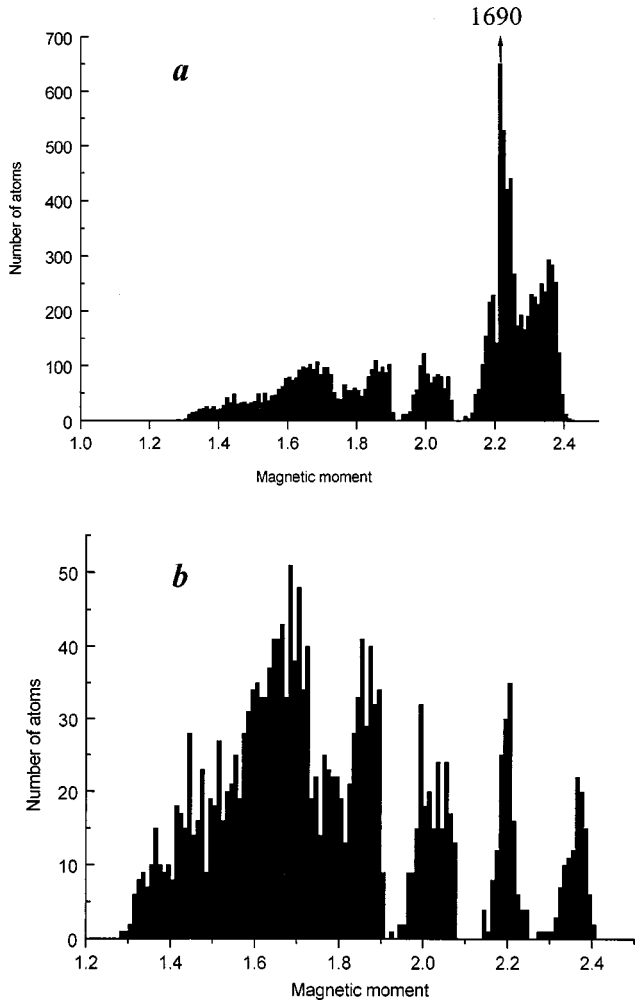

FIG. 11. Calculated distribution of magnetic moments (in μ_B) of Fe atoms for a smooth interface: (a) 3-ML-thick layers for both interfaces; (b) 1-ML-thick layer for the Cr/Fe interface (Cr on Fe interface).

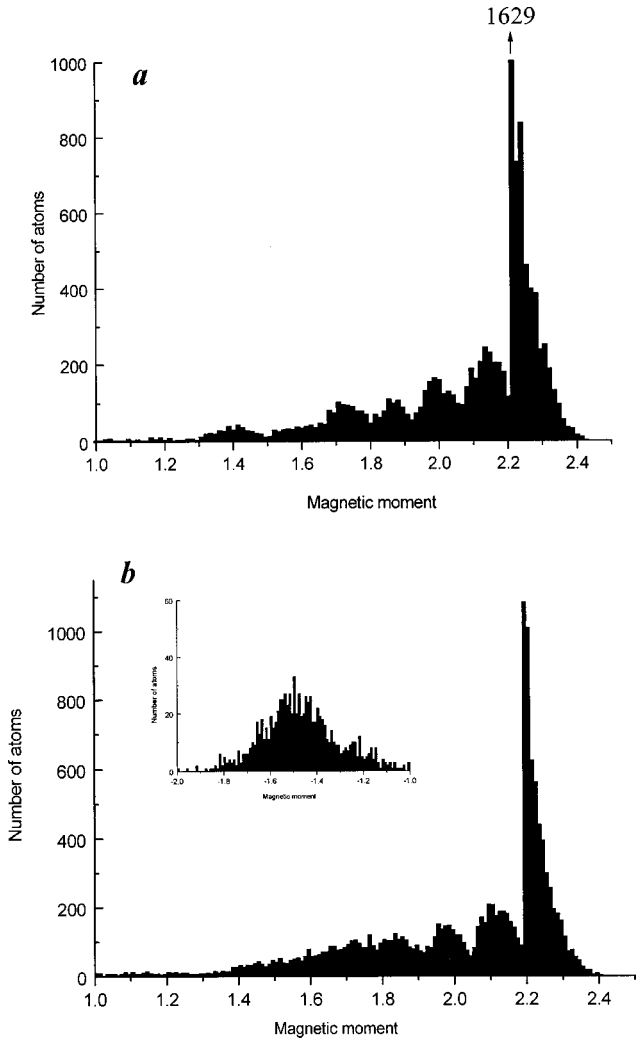

FIG. 12. Calculated distribution of magnetic moments (in μ_B) of Fe atoms from 3 ML at the interface with interdiffusion: (a) rough, (b) rough+alloy. The inset shows the distribution of moments of Fe atoms opposite to the overall magnetization direction.

computations based on the Hubbard-like tight-binding model[20] for the special cases of ordered structures, which were considered there. In our calculations we do not reproduce peaks in the distribution of magnetic moments corresponding to small hff magnitudes less then 20 T. Note that the satellite with hff $B_{\rm hf}^*=19$ to 20 T was associated in previous studies[9,11 and 13–15] with Fe atoms in the ''flat'' interface ($B_{\rm hf}^*=23$ T in Ref. 10). Correspondingly, the increase of its amplitude in the Mössbauer spectra, which takes place in particular by raising the substrate temperature during the sample preparation or by annealing, was interpreted as smoothing of the interface.[15] The number of ^{57}Fe atoms with this hff can be larger then the number of ^{57}Fe atoms with other field values, especially in the case of one monolayer of ^{57}Fe at the interface. Note, however, that in the case of one-monolayer high-stepped interfaces with average step width $N_{\rm st}$ the number of Fe atoms in ''flat interface'' positions should be $N_{\rm sf}-1$ times larger than the number of step edge or kink positions. Even for relatively narrow steps ($N_{\rm st}\cong 20$) such a relation between the amplitude at $B_{\rm hf}^*$ and that of other lines with higher fields in the hff distribution was never observed in CEMS spectra. The calculated value of the Fe moment at the flat interface (about $1.7\mu_B$) proves to be essentially higher than the moment $M^*=[B_{\rm hf}^*/B_{\rm hf}({\rm bulk})]M_{\rm bulk}$ of about $1.3\mu_B$, which corresponds to the hff $B_{\rm hf}^*$. If we accept the proportionality of magnetic moment and hff (Ref. 39), which is suggested by Fig. 1, the field $B_{\rm hf}^*$ is associated with Fe atoms that have a larger number of Cr neighbors than those in ''flat'' interfaces and, consequently, must lie inside of Cr spacer layers a few monolayers away from the ideal interface. Then, a large amplitude of the satellite with $B_{\rm hf}^*$ cannot be a signature of the atomically smooth (''flat'') interface, but, to the contrary, indicates alloying and interdiffusion near the interface. The absence of maxima in the moment distribution around M^* in our calculations can be explained by the following reason: we considered only structures where Fe atoms cannot penetrate too far from the interface. Only the rough+alloy structure contained Fe atoms inside the Cr spacer, in particular, in the state 8/6. However, in this case Fe atoms effectively interact through

the Cr atoms, because, as is seen from Fig. 10, they strongly polarize Cr moments. It is worth mentioning that we perform our calculations for zero temperature, whereas most Mössbauer (CEMS) measurements were made at room temperature. Fe atoms with their local moments being reduced by the Cr surrounding at a first glance seem to be much more sensitive to the influence of temperature than bulk Fe moments, especially taking into account that room temperature is not very far from the Neel temperature of (bulk) Cr. However, we have also performed CEMS at 80 K, and these results did not show a significant difference in the hff distributions measured at 300 or 80 K. In particular, $B_{\rm hf}^{*}$ values at 300 K (19.7 T) and at 80 K (20.9 T) were observed to be nearly the same. Therefore, these ''loose spins,'' [4] associated with field $B_{\rm hf}^{*}$, even if they have configuration 8/6, lie very close to the interface and essentially differ from the paramagnetic Fe impurities in the bulk Cr.

The conclusion that the hff $B_{\rm hf}^{*}$ is associated with Fe atoms inside the Cr spacer (a few ML away from the ideal interface) leads to some important consequences related to the mechanisms of epitaxial growth of Fe on Cr (Fe/Cr) and Cr on Fe (Cr/Fe), which are in contradiction with the traditional model. Mössbauer studies[24] show that for probe ^{57}Fe layers at the Fe/Cr interface (''lower'') the amplitude of the $B_{\rm hf}^{*}$ satellite is enhanced in comparison with that of the Cr/Fe interface (''upper''). In the spirit of the traditional model[9,11 and 13–15] this was interpreted as evidence for suppressed intermixing during Fe growth on a Cr substrate.[24] However, according to our present result the interpretation must be reverse. Such an asymmetry of two interfaces can be understood from simple thermodynamic considerations.[40] Interface alloying may be governed by the binding energy between the substrate and ad-atom material, which are proportional to the melting points of the solids. The melting point of Cr (2130 K) is higher than for Fe (1808 K) and, therefore, interface mixing for the Fe/Cr interface (''lower'') might be suppressed. For certain interfaces these simple considerations were checked experimentally.[41,42] However, in some cases they are not valid. For example, in Ref. 43 surface alloying of Au on Ni was reported, when the melting point of the substrate (1728 K for Ni) essentially exceeds the melting point of the ad atom (1337 K for Au) and, moreover, Au and Ni are immiscible metals. For a theoretical analysis of the intermixing process on the microscopic level proper allowance must be made for changes of magnetic properties and the related energy due to exchange of the atoms at the interface as well as to the effects of interface roughness.

In Ref. 44 calculations based on the local-density functional theory and the Korringa-Kohn-Rostoker (KKR)-Green-function method demonstrate a strong tendency for a direct site-exchange mechanism into the first surface layer for Cr on the ideal Fe surface (Cr/Fe or upper interface). There is no similar calculation for Fe on Cr due to the complex spin-density-wave structure of bulk Cr and the necessity to take into account its modification by the surface and adsorbed Fe atoms. In addition, a nonideal Fe/Cr interface forms noncollinear magnetic structures,[23,36,44,45] which also can be important for the calculation of the energy balance for the intermixing process.

There are, however, some experimental indications that alloying cannot be avoided even for Fe growth on Cr, although the specific scenarios of intermixing on Fe/Cr and Cr/Fe interfaces can be different. As was noted by Heinrich *et al.*,[2,40] scanning electron microscopy with polarization analysis (SEMPA) and Brillouin light scattering (BLS) show that the phase of the short-wavelength oscillations in the interlayer coupling for Fe whisker/Cr/Fe(001) structures is exactly opposite to that expected from AF coupling for Fe-Cr and Cr-Cr layers. This was explained by interdiffusion at the Fe/Cr interface, and recent calculations of Freyss, Stoeffler, and Dreysse[20] confirmed the possibility of changing the exchange coupling phase for the ordered interface structure with two intermixed layers $Cr_xFe_{1-x}/Cr_{1-x}Fe_x$ for $x \geqslant 0.2$. For one mixed layer the calculations gave a phase change only for a higher degree of intermixing: a mixed layer with iron concentration less than 50 at. % behaves like a pure Cr atomic layer. This last conclusion, however, was not in agreement with experiments,[40] where it was shown that introduction of one mixed Cr85%-Fe15% layer instead of one Fe layer does not change the phase of the interlayer coupling. This contradiction between theory and experiment can be explained, if we accept interdiffusion at the Fe/Cr interface. In this case the interface Cr layer contained Fe atoms already without artificial alloying, and additional 15 at. % in concentration change can be crucial for the sign of interlayer exchange coupling. Note also that losing some Fe atoms through the interface to the Cr spacer can change the effective thickness of Fe and Cr layers, and also may cause the phase change observed in SEMPA and BLS experiments. Note also that a direct proof by STM of the surface alloy formation of Fe on Cr was reported recently by Choi *et al.*[6]

For the interdiffusion process the temperature of the epitaxial growth is very important. SEMPA studies[46] demonstrate that with increase of the substrate temperature a transition from a three-dimensional to a layer-by-layer growth mode takes place. At the same time the temperature rise leads to more intense diffusion at the interface. In Ref. 47, by using high-resolution low-energy electron diffraction and Auger electron spectroscopy, it was found that interdiffusion is responsible for the interface roughness, when the growth temperature exceeds 400 K. A recent study of the growth of a thin Fe layer on Cr by means of reflection high-energy electron diffraction (RHEED) shows that the largest number of RHEED intensity oscillations was observed at the lowest growth temperature.[48] For an explanation of this phenomenon a special scenario was developed in Ref. 48, which is based on the special form of interface roughness with steps higher then one monolayer, although probably alloying at the interface (which was excluded from the model) plays an important role here.

New information about changes of the interface structure can be given by Mössbauer studies after thermal treatment. In Ref. 15 Fe/Cr multilayers were annealed for 1 h at temperatures of 200–450 °C. The authors essentially observed a weak increase in amplitude of the hff $B_{\rm hf}^{*}=20$ T after annealing at 300 °C. Their interpretation is based on the supposition that the field $B_{\rm hf}^{*}$ corresponds to Fe atoms in the ''flat'' interface. In this case they had to conclude that there is in-

plane diffusion inside the superlattice during annealing that leads to smoothing of the interfaces. This is an unlikely process, however. If, however, B_{hf}^{*} corresponds to the Fe atoms in the Cr spacer a few atomic layers away from the ideal interface, such a behavior can be explained in a much more natural way: simply increasing the degree of intermixing at the annealing temperature.

Note also that our calculation gives a new criterion for determining the quality of the interface roughness: it is the appearance of the enhanced hff near 34 T that evidences the atomically flat interface via the hff of the (0, 1) subsurface Fe site. However, its observation is a much more complicated problem than the field B_{hf}^{*} and can be done only on particularly prepared samples, where the roughness is artificially suppressed.[10]

VI. CONCLUSIONS

We performed measurements of the magnetic hyperfine field (hff) in Fe/Cr(001) superlattices with different thicknesses of ^{57}Fe probe layers at the interface, and we made self-consistent calculations of the atomic magnetic moment in the interface region for the same multilayer structure. Different kinds of interface roughnesses were modeled using special algorithms. We obtain a strong correlation between the ^{57}Fe hff measured by CEMS and local Fe magnetic moments calculated within PAM. Peak positions of satellites in the CEM spectra and positions of maxima in the distribution function for local magnetic moments prove to be stable relative to changes in the alloylike interface roughness.

For every kind of interface roughness we calculated the distribution of local moments among the Fe atoms with a given number of nearest and next-nearest Cr neighbors. These dependencies show that the assumption of an additive influence of Cr neighbors on the Fe magnetic moment fails for multilayers on a microscopic level, but can be valid in the average for a random alloy.

We found that the hff of $B_{\mathrm{hf}}^{*}\approx 20$ T corresponds to interdiffused Fe atoms inside the Cr spacer layers (but not far away (i.e., $\sim$2–4 ML) from the interface), contrary to the traditional interpretation of Fe atoms at the atomically ''flat'' interface. For atomically smooth interfaces with large flat terraces an enhanced hff must be observed in the second Fe layer below the ideal interface, and it can provide a measure of the Fe-Cr interface roughness on an atomic scale. For instance, knowledge of the latter quantity is of fundamental importance for the understanding of the origin of magnetoresistance (bulk or interface scattering[14,49–51]) in Fe-Cr heterostructures.

ACKNOWLEDGMENTS

Valuable technical assistance by U. von Hörsten is highly appreciated. We are particularly grateful to Dr. Chr. Sauer (Jülich) for enlightening discussions, and to Dr. J. S. Jiang (Argonne) for some of the XRD measurements. This work was supported by INTAS (Grant No. 96-0531), the ''Universities of Russia'' Grant No. 992780, and Deutsche Forschungsgemeinschaft (SFB 491 Bochum/Duisburg). V.M.U. would like to express his gratitude to the Alexander von Humboldt-Stiftung for financial support.

[1] H. Zabel, J. Phys.: Condens. Matter **11**, 9303 (1999).
[2] B. Heinrich, J. F. Cochran, D. Venus, K. Totland, D. Atlan, S. Govorkov, and K. Myrtle, J. Appl. Phys. **79**, 4518 (1996).
[3] C. Turtur and G. Bayreuther, Phys. Rev. Lett. **72**, 1557 (1994); S. Miethaner and G. Bayreuther, J. Magn. Magn. Mater. **148**, 42 (1995).
[4] J. C. Slonczewski, J. Magn. Magn. Mater. **150**, 13 (1995).
[5] D. T. Pierce, J. Unguris, R. J. Celotta, and M. D. Stiles, J. Magn. Magn. Mater. **200**, 290 (1999); A. Davies, J. A. Stroscio, D. T. Pierce, and R. J. Celotta, Phys. Rev. Lett. **76**, 4175 (1996).
[6] Y. J. Choi, I. C. Jeong, J.-Y. Park, S.-J. Kahng, J. Lee, and Y. Kuk, Phys. Rev. B **59**, 10 918 (1999).
[7] R. Pfandzelter, T. Igel, and H. Winter, Phys. Rev. B **54**, 4496 (1996).
[8] D. Venus and B. Heinrich, Phys. Rev. B **53**, R1733 (1996).
[9] J. Landes, Ch. Sauer, R. A. Brand, W. Zinn, and Zs. Kajcsos, Hyperfine Interact. **57**, 1941 (1990); J. Landes, Ch. Sauer, R. A. Brand, W. Zinn, S. Mantl, and Zs. Kajcsos, J. Magn. Magn. Mater. **86**, 71 (1990); J. Landes, Ch. Sauer, S. Dörrer, and W. Zinn, *ibid.* **113**, 137 (1992).
[10] F. Klinkhammer, Ch. Sauer, E. Yu. Tsymbal, S. Handschuh, Q. Leng, and W. Zinn, J. Magn. Magn. Mater. **161**, 49 (1996).
[11] D. L. Williamson, B. M. Lairson, A. P. Payne, N. M. Rensing, and B. M. Clemens, Hyperfine Interact. **92**, 1271 (1994); N. M. Rensing, B. M. Clemens, and D. L. Williamson, J. Appl. Phys. **79**, 7757 (1996).
[12] J. Zukrowski, G. Liu, H. Fritzsche, and U. Gradmann, J. Magn. Magn. Mater. **145**, 57 (1995).
[13] H. Schrör, W. Keune, N. Hosoito, and T. Shinjo, *Digest of the 15th International Colloquium on Magnetic Films and Surfaces (ICMFS'97) Sunshine Coast, Australia, July 1997* (unpublished).
[14] R. Schad, P. Belien, G. Verbanck, K. Temst, H. Fischer, S. Lefebvre, M. Bessiere, D. Bahr, J. Falta, J. Dekoster, L. Langouche, V. V. Moshchalkov, and Y. Bruynseraede, J. Magn. Magn. Mater. **198**, 104 (1999); R. Schad, P. Belien, G. Verbanck, K. Temst, V. V. Moshchalkov, Y. Bruynseraede, B. Bahr, J. Falta, J. Dekoster, and G. Langouche, Europhys. Lett. **44**, 379 (1998).
[15] M. Kopcewicz, T. Lucinski, F. Stobiecki, and G. Reiss, J. Appl. Phys. **85**, 5039 (1999).
[16] T. S. Toellner, W. Sturhahn, R. Röhlsberger, E. E. Alp, C. H. Sowers, and E. E. Fullerton, Phys. Rev. Lett. **74**, 3475 (1995).
[17] A. J. Freeman and R. Wu, Nuovo Cimento D **18**, 137 (1996); J. Magn. Magn. Mater. **100**, 497 (1991).
[18] S. M. Dubiel and J. Zukrowski, J. Magn. Magn. Mater. **23**, 214 (1981).
[19] R. Coehoorn, J. Magn. Magn. Mater. **151**, 341 (1995).
[20] M. Freyss, D. Stoeffler, and H. Dreysse, Phys. Rev. B **56**, 6047 (1997).

[21] A. K. Kasansky and V. M. Uzdin, Phys. Rev. B **52**, 9477 (1995).
[22] V. Uzdin, D. Knabben, F. U. Hillebrecht, and E. Kisker, Phys. Rev. B **59**, 1214 (1999); V. Uzdin, D. Knabben, F. U. Hillebrecht, and E. Kisker, J. Magn. Magn. Mater. **198–199**, 680 (1999).
[23] D. Knabben, Th. Koop, H. A. Dürr, F. U. Hillebrecht, and G. van der Laan, J. Electron Spectrosc. Relat. Phenom. **86**, 201 (1997).
[24] T. Shinjo and W. Keune, J. Magn. Magn. Mater. **200**, 598 (1999).
[25] W. Sturhahn, R. Roehlsberger, E. E. Alp, T. Ruckert, and W. Keune, J. Magn. Magn. Mater. **198–199**, 590 (1999).
[26] R. A. Brand, Nucl. Instrum. Methods Phys. Res. B **28**, 398 (1987); the NORMOS program is available from Wissel GmbH, D-82319 Starnberg, Germany.
[27] J. Hesse and A. Rübartsch, J. Phys. E **7**, 526 (1974).
[28] C. Orme and B. G. Orr, Surf. Rev. Lett. **4**, 71 (1997).
[29] A. L. Barbas, H. E. Stanley, *Fractal Concepts in Surface Growth* (Cambridge U.P., Cambridge, 1995).
[30] M. S. Borczuch and V. M. Uzdin, J. Magn. Magn. Mater. **172**, 110 (1997).
[31] C. Demangeat and V. M. Uzdin, J. Magn. Magn. Mater. **156**, 202 (1996).
[32] V. M. Uzdin and N. S. Yartseva, Comput. Mater. Sci. **10**, 211 (1998).
[33] V. M. Uzdin and C. Demangeat, J. Magn. Magn. Mater. **165**, 458 (1997).
[34] A. Vega, L. C. Balbas, and G. M. Pastor, Phys. Rev. B **50**, 3899 (1994).
[35] V. N. Gittsovich, V. G. Semenov, and V. M. Uzdin, J. Magn. Magn. Mater. **146**, 165 (1995).
[36] V. M. Uzdin, N. S. Yartseva, A. Mokrani, and C. Demangeat, J. Magn. Magn. Mater. **198–199**, 471 (1999); V. M. Uzdin, N. S. Yartseva, and S. A. Yartsev, *ibid.* **196–197**, 70 (1999).
[37] N. S. Yartseva, V. M. Uzdin, and C. Demangeat, Comput. Mater. Sci. **10**, 255 (1998).
[38] Z. Li and H. Luo, J. Phys.: Condens. Matter **3**, 9141 (1991).
[39] Full potential linearized augmented plane wave (FLAPW) calculations have led to the theoretical discovery that the local Fe moment, μ, and the hff, B_{hf}, may fail to be proportional at *ideally flat* surfaces and interfaces, contrary to the bulk behavior [A. J. Freeman and R. Wu, J. Magn. Magn. Mater. **100**, 497 (1991), and references therein]. For Fe/Cr interfaces such calculations do not exist. However, the concept of atomically flat interfaces used in the theoretical work is realized only in very few systems. The loss of proportionality between μ and B_{hf} has been experimentally verified only on two MBE-grown systems, i.e., bcc-Fe(110)/vacuum and W(110)/Fe(110) interfaces [U. Gradmann, *ibid.* **100**, 481 (1991), and references therein]. However, as is discussed in Ref. 24, the theoretically predicted effects seem to be suppressed by interface roughness and interdiffusion at real interfaces (like in the present Fe/Cr samples), and the proportionality of μ and B_{hf} then seems to be restored, as suggested also by the correlation observed in Fig. 1.
[40] B. Heinrich, J. F. Cochran, T. Monchesky, and K. Myrtle, J. Appl. Phys. **81**, 4350 (1997); B. Heinrich, J. F. Cochran, T. Monchesky, and R. Urban, Phys. Rev. B **59**, 14 520 (1999).
[41] Th. Detzel and N. Memmel, Phys. Rev. B **49**, 5599 (1994).
[42] P. J. Schurer, Z. Celinski, and B. Heinrich, Phys. Rev. B **51**, 2506 (1995).
[43] L. P. Nielsen, F. Besenbacher, I. Stensgaard, E. Laegsgaard, C. Engdahl, P. Stoltze, K. W. Jakobsen, and J. K. Norskov, Phys. Rev. Lett. **71**, 754 (1993).
[44] B. Nonas, K. Wildberger, R. Zeller, and P. H. Dederichs, Phys. Rev. Lett. **80**, 4574 (1998).
[45] G. Panaccione, F. Sirotti, E. Narducci, and G. Rossi, Phys. Rev. B **55**, 389 (1997).
[46] D. T. Pierce, J. A. Stroscio, J. Unguris, and R. J. Celotta, Phys. Rev. B **49**, 14 564 (1994).
[47] J. Schwabenhausen, T. Dürkop, and H.-J. Elmers, Phys. Rev. B **55**, 15 119 (1997).
[48] K. Theis-Bröhl, I. Zoller, P. Bödeker, T. Schmitte, H. Zabel, L. Brendel, M. Belzer, and D. E. Wolf, Phys. Rev. B **57**, 4747 (1998).
[49] E. E. Fullerton, D. M. Kelly, J. Guimpel, I. K. Schuller, and Y. Bruynseraede, Phys. Rev. Lett. **68**, 859 (1992).
[50] S. S. P. Parkin, Phys. Rev. Lett. **71**, 1641 (1993).
[51] P. Zahn, J. Binder, I. Mertig, R. Zeller, and P. H. Dederichs, Phys. Rev. Lett. **80**, 4309 (1998).